

# MULTIFREQUENCY RADIO OBSERVATIONS OF THE CRAB PULSAR

David A. Moffett<sup>1,2</sup> and Timothy H. Hankins<sup>3</sup>

Physics Department, New Mexico Institute of Mining and Technology  
Socorro, NM 87801

## ABSTRACT

Previously unseen profile components of the Crab pulsar have been discovered in a study of the frequency-dependent behavior of its average pulse profile between 0.33 and 8.4 GHz. One new component, 36° ahead of the main pulse at 1.4 GHz, is not coincident with the position of the precursor at lower frequencies. Two additional, flat-spectrum components appear after the interpulse between 1.4 and 8.4 GHz. The normal interpulse undergoes a transition in phase and spectrum by disappearing near 2.7 GHz, and reappearing 10° earlier in phase at 4.7 and 8.4 GHz with a new spectral index. The radio frequency main pulse disappears for  $f > 4.9$  GHz, even though it is seen at infrared, optical, and higher energies. The existence of the additional components at high frequency and the strange, frequency-dependent behavior is unlike anything seen in other pulsars, and cannot easily be explained by emission from a simple dipole field geometry.

*Subject headings:* pulsars: individual(PSR 0531+21) — stars: neutron

## 1. Introduction

Since its discovery (Staelin & Reifenstein 1968, Comella et al. 1969), the Crab Nebula pulsar has been studied at many wavelengths, including optical, X-ray and  $\gamma$ -rays, to understand the properties of the emission mechanism. Radio emission from the Crab pulsar is unusual because of its giant pulses, which are very powerful intensity fluctuations varying from 100 to 1000 times the mean intensity that occur at random intervals from one pulse to several thousand pulse periods. But the pulsar's steep radio spectrum and the radio-bright Crab Nebula background make

---

<sup>1</sup>also National Radio Astronomy Observatory, P.O. Box O, Socorro, NM 87801

<sup>2</sup>Electronic mail: dmoffett@nrao.edu

<sup>3</sup>Electronic mail: thankins@nrao.edu

observations above 1 GHz difficult with single dish antennas. Average profiles formed at 4.7 GHz during the single successful observation in a decade of attempts at the Arecibo 305-m telescope, revealed that the main pulse (MP) to interpulse (IP) separation appeared to be smaller than at longer wavelengths, and that additional pulse profile components were present following the IP. To investigate this atypical frequency-dependent behavior of the pulse profile and to overcome the background contribution of the Nebula, the observing program was continued at the Very Large Array (VLA) of the National Radio Astronomy Observatory.

## 2. Observations

A series of observations of the Crab pulsar were made between February 9 and May 27, 1994 at 0.33, 1.4, 4.9, and 8.4 GHz with the VLA in its phased-array mode. The antenna peculiar phases are determined by observing an extragalactic continuum point source calibrator and then applied in real time to synthesize a pencil beam on the sky. Using this aspect of the interferometer, the longer spatial wavelengths of the bright Crab Nebula supernova remnant are resolved. Consequently, when observing the Crab pulsar with the VLA, the effective system temperature is that of a single 25-meter dish, but with the collecting area for a point source equivalent to a 130-meter dish. At the VLA the signal-to-noise ratio of the Crab pulsar is therefore greater than for the Arecibo telescope by approximately the inverse ratio of the element areas, or  $(305\text{ m} / 25\text{ m})^2$ .

When operating in the VLA's phased-array mode, the received voltages from each antenna are appropriately delayed, then sampled, summed, and re-converted to an "Analog Sum", which represents the analog voltage from the synthesized pencil beam. During our observations, the left- and right-circularly polarized Analog Sum signals were sent to a MkIII VLBI Video Converter, which can be used as a dual 14-channel filter bank with bandwidths adjustable in octave steps from 0.125 to 4 MHz. The filter bank is followed by a set of square-law detectors with adjustable integration time constants and DC offsets. The channel bandwidths and detector time constants were selected to optimize the time resolution afforded by dispersion smearing. We utilized the Princeton/Dartmouth Mark III Pulsar Timing System (Stinebring *et al.* 1992) to sample and record 14 frequency channels of the left- and right-circularly polarized signals. To fold the incoming data at the topocentric period, we utilized the monthly timing models published by Lyne & Pritchard (1994) and the program TEMPO (Taylor & Weisberg 1989) to generate the topocentric period for each of our observing sessions as input to the timing system. Each scan was two minutes long, during which an average profile was created and saved with a precise time stamp of the scan. The observed profile consists of 1024 numbers representing the relative flux density throughout the entire pulsar rotation period. The timing system clock was referenced to the station standard clock, and was started by a ten-second tick referenced to UTC through a GPS receiver.

Pulsed emission was easily detected at 0.33 and 1.4 GHz, but emission at 4.9 and 8.4 GHz was strongly variable and not detected for all the observing sessions. Significant emission at 4.9 GHz was detected only during four of nine sessions of 3-hour duration. Detection of 8.4 GHz emission occurred only on two sessions. During the times when the average profile was seen in a two-minute average, individual “giant” pulses could easily be seen on a synchronized oscilloscope (Hankins & Moffett 1996). The typical interval over which the pulsar could be seen above the noise level at 8.4 GHz was 10 to 30 minutes, and these did not often repeat in a single observing session. Unfortunately, we could not observe separate frequencies simultaneously, and so we cannot make quantitative estimates as to how long the emission was absent during a session, since our procedure was to search at other frequencies if detectable emission could not be found after 10 to 20 minutes. On one occasion at 8.4 GHz, pulses occurred in bursts where a pulse was seen in nearly every period for up to a minute. We tentatively attribute this effect to diffractive interstellar scintillation, which is usually associated with short time-scale intensity fluctuations.

### 3. Timing Analysis

Total intensity profiles were formed by adding two minute average profiles from each filter bank channel after accounting for the appropriate dispersion measure delay between channels. Each profile thus summed was cross-correlated with a high signal-to-noise standard profile, or *template*, to determine the phase and ultimately the time of arrival of the pulsar waveform with respect to a reference or *fiducial* point on the template. At 0.33 and 1.4 GHz, the signal-to-noise ratio was high enough that the respective templates could be formed from stacked scans. At 4.9 and 8.4 GHz, the signal-to-noise was low, so a Gaussian template was used for these frequencies. Since the waveform of the Crab is frequency dependent, the templates were aligned to the centroid of the main pulse. However the main pulse was not a suitable fiducial point at 8.4 GHz, and so its alignment with the other frequencies was constrained by the timing model and the dispersion measure. Because of the instrumental smoothing response of the detectors, the position of the MP at 0.33 and 1.4 GHz was determined after deconvolving a model of the detector response function.

After observing, we used the same input timing models of Lyne & Pritchard (1994) to compare with the actual times of arrival (TOA) from our scans. The standard deviation of our timing residuals for any single session was on the order of  $4\mu\text{s}$  at 1.4 GHz, which is considerably smaller than the standard deviation of the residuals from the average time of arrival from each day. The residuals from 4.9 and 8.4 GHz were higher, from 15 to  $40\mu\text{s}$ . Since the signal-to-noise was low for the higher frequencies, we attribute the scatter of 4.9 and 8.4 GHz residuals from a single session to estimation error from radiometer noise. Shifts of 50 to  $100\mu\text{s}$  in the 1.4 GHz arrival times were found to occur from one session to the next. Such jumps have been seen in optical and radio timing observations of the Crab (Boynton et al. 1972, Groth 1975, Lyne, Pritchard, & Smith 1988), and have been described as “timing noise”. In a study of the timing noise phenomenon,

Cordes (1980) found the process to be a random walk process on short time-scales; but over longer periods of time, Lyne, Pritchard, & Smith (1988) found that the deviation in arrival times has a quasi-sinusoidal component with a 20-month period whose amplitude varies from 5 to 10 milliseconds. Over our short observing term, our arrival time deviations would show no evidence of this periodic component, and the arrival times from one observing session to the next would appear to be random.

Solutions for dispersion measure were made from individual multifrequency observation sessions. During a session from February 22 to 23, three frequencies were observed and the dispersion measure (DM) found during this session was  $56.826 \pm 0.010 \text{ pc-cm}^{-3}$ , which agrees with Lyne & Pritchard's average value of  $56.827 \pm 0.005 \text{ pc-cm}^{-3}$  for February 1995. Other determinations were made from observations at 1.4 and 4.9 GHz on February 14 and 19, and May 14. No significant departures of DM from Lyne & Pritchard's models for February and May were found beyond three times the estimated error of  $0.01 \text{ pc-cm}^{-3}$ , and there is no evidence for superdispersion delay. After removing the time delay for a fixed DM, the profiles from 0.33, 1.4, and 4.9 GHz were found to align at the position of the main pulse, which was chosen earlier as the reference point for determining the arrival time of the averaged pulses. The 8.4 GHz profile was found to align with other profile components seen at 4.9 GHz.

#### 4. Multifrequency Properties

Figure 1 shows the aligned, average profiles recorded at 0.33, 1.4, 4.9, and 8.4 GHz with the phased VLA. The amplitude scale at each frequency was estimated from the off-pulse radiometer noise, antenna and receiver parameters, integration time, and expected contribution from the Crab Nebula.

In the 0.33 GHz profile one can see the precursor, MP and IP. The precursor and MP overlap, due to a dispersion broadening of 1.6 ms across the 0.125 MHz bandwidth filters and a 1-ms detector time constant. One feature to note is a broad non-zero component or *emission bridge* between the MP and IP, which has been detected previously by Rankin *et al.* (1970) at 196.5 MHz, by Manchester, Huguenin, & Taylor (1972) at frequencies from 114 to 159 MHz, and by Vandenberg *et al.* (1973) at 111.5 and 196 MHz. The estimated flux density of the average profile is 0.88 Jy, nearly the same as estimated from the spectrum compiled by Sieber (1973).

At 1.4 GHz, the precursor has vanished due to its steep spectral index, leaving only the MP, IP, and a weak but distinct low-frequency component  $\sim 36^\circ$  ahead of the MP (which we will refer to as LFC). The appearance of this component, distinct from the precursor, has been verified by observations at 608 and 1400 MHz (Lyne & Pritchard 1995), and can be seen as a slight rise above the noise level at 4.8 GHz. This new component may be present at 0.33 GHz, but better time resolution would be required to separate it from the precursor. The estimated integrated flux

density of this profile is 6.3 mJy; only half of the expected value.

At 4.9 GHz, the profile becomes quite complex. The profile clearly shows four components despite the lower signal-to-noise ratio. Since our profiles are aligned, we identify the first two narrow components as the MP and IP. The two broader components (which we will refer to as HFC1 and HFC2) following the IP have similar pulse energies at 4.9 and 8.4 GHz, indicating that they are nearly flat-spectrum components. They are coincident in pulse phase with the weak features appearing in the 1.4 GHz profile. Another striking feature of this profile is that *the IP appears to shift earlier in phase*. Both the shift and the existence of additional components confirm the 4.7 GHz profile recorded in 1981 at the Arecibo telescope (see Figure 2). The integrated flux from our estimate is 0.47 mJy, only slightly higher than expected (0.35 mJy).

In the 8.4 GHz profile, the main pulse disappears altogether. The estimated spectrum from 0.33 to 4.9 GHz suggests that the main pulse has dropped below the noise level. However, the apparent interpulse seems to have become more energetic from 4.9 to 8.4 GHz. Our estimate of the flux density at 8.4 GHz is 0.61 mJy, 10 times that extrapolated from lower frequencies. An independent continuum observation at 8.4 GHz by Frail (1995) has placed the flux density of the pulsar at  $0.5 \pm 0.1$  mJy. Thus the spectrum of the pulsar seems to become flatter at high frequencies.

In Figure 2 we have plotted the VLA profiles in a summary of normalized waveforms from other radio frequencies and energy bands. Profiles at 0.43, 0.6, 2.7 and 4.7 GHz were obtained from Arecibo and Effelsberg archival data recorded by Hankins. Though the VLA profiles are aligned after removing dispersion delay, all other profiles in the figure have been arbitrarily aligned by the peak of the main pulse only. We note, that radio and higher energy waveforms observed by other authors have been shown to align absolutely as in the figure.

By comparing all these profiles, we can identify even more properties. The LFC can be seen from 0.6 to 4.8 GHz, just barely above the noise level at some frequencies. At 2.7 GHz, the interpulse disappears, then it reappears at 4.7 GHz,  $\sim 10^\circ$  ahead of its low frequency position. Then between 8.4 GHz and  $2.2 \mu\text{m}$ , the profile evolves from having only three components, with the main pulse missing, back to two components, with much broader MP and IP. Though the MP and IP dominate emission in the infrared, we note the existence of a small rise of emission after the interpulse, in the same region of phase as radio components HFC1 and HFC2. At higher energies, the shape of the MP and IP remains virtually constant, with a bridge of emission between the two, similar to the radio emission bridge seen at 0.33 GHz.

Gaussian waveforms were fitted to the relative positions of the profile components in order to find the width and phase separation of components with frequency. The half-power widths of the precursor and HFC2 are comparable, while the width of the interpulse was found to increase monotonically with frequency. The decrease of  $\Delta\phi_{\text{MP-IP}}$  is suggestive of a radius-to-frequency mapping phenomenon that has been seen in profiles of conal pulsars (Cordes 1978, Hankins & Fowler 1986, Thorsett 1991), but the discontinuous jump of  $\Delta\phi_{\text{MP-IP}}$  from 1.4 to 4.7 GHz is

not consistent with the smooth change with frequency in component separation found for conal pulsars.

## 5. Discussion

The appearance of additional profile components at high radio frequencies (and possibly IR) and the change of profile morphology between radio and higher energies further complicates the problem of where the Crab pulsar's emission originates and how it is generated. The average profiles presented here are not typical of other pulsar profiles; there are up to six different regions in pulse phase where emission occurs. Of the millisecond pulsars, one is known to have more components, PSR J0437-4715, with up to 8 components or more (Manchester & Johnston 1995). Though not rotating as fast, the Crab's velocity-of-light cylinder is still relatively close to the surface, where multipole fields may exist (Kuz'min 1992). The HFC components seen at 4.7, 4.9 and 8.4 GHz, and the third component at  $2.2\mu\text{m}$  in Figure 2 may stem from emission originating in multipole fields near the star's surface.

The discovery at 1.4 GHz of the LFC component leading the MP at nearly twice the phase separation of the MP and precursor might be evidence for a core/cone set. The half-power widths of the precursor at 0.33, 0.43, and 0.6 GHz are the same as core component widths predicted from the empirical core width-period relationship established by Rankin (1993) for a near orthogonal rotator. Also, the LFC-to-MP separation is almost the same as the inner conal diameter predicted by Rankin for a pulsar of this period. The steeper spectrum of the precursor relative to the LFC also supports their interpretation as core and cone components, respectively. But then if we interpret the LFC-MP pair as conal components (with similar spectral indices), we must rationalize their dramatically unsymmetric amplitudes. On the other, if the MP is not one of a conal component pair, but originates in the outer magnetosphere, then the lagging conal component mate of the LFC may just be buried under the MP.

The disappearance of the MP at 8.4 GHz should not surprise us. If the spectral index remains constant between 0.33 and 4.9 GHz, then the MP should lie below the noise level at 8.4 GHz. We have seen giant pulses from the MP at this frequency, but when averaged in time, no component appears. For it to reappear at higher energies, both the beam and the emission mechanism must make a significant change. The IP does undergo a transition within the range of radio frequencies observed here. The spectral index from 0.33 to 1.4 GHz suggests that it should be spectrally dead by 4.7 GHz. The lack of an IP at 2.7 GHz tends to support this despite the profile's modest signal-to-noise. The apparent IP at  $\nu \geq 4.7\text{ GHz}$  could very well be a *new component*, much like the other HFCs, with a different spectral index from that of the low-frequency IP.

The high frequency components, HFC1 and HFC2, appear from 1.4 GHz to 8.4 GHz, and perhaps contribute to emission seen in the IR at  $2.2\mu\text{m}$ . They have a flatter spectrum than the

MP and IP, and at high frequency they dominate the profile, tending to flatten the spectral index of the pulsar. This property has been seen in other pulsars at high frequency (Wielebinski *et al.* 1993) and for the Crab this should hold true – because the energy spectrum between the radio and IR band has a large discontinuity which could only be accounted for by a turn-up of the spectrum (see figure 4–2, Manchester & Taylor 1977).

We can make no interpretation of the magnetic field geometry from the pulse morphology without full polarization information. Weak linear polarization in both the MP and IP was found in observations by Manchester, Huguenin, & Taylor (1972) between 110 and 160 MHz and by Manchester (1971) at 430 and 1400 MHz. And the precursor is well known to be strongly polarized. However, no significant sweep in polarization position angle was found across the precursor, MP and IP. If the rotating vector model of Radhakrishnan and Cooke (1969) holds true, then the lack of position angle variation suggests that emission may be from one pole as it sweeps across the line of sight. However the optical polarization position angle sweep (Kristian *et al.* 1970) suggests that emission comes from two poles (Narayan & Vivekanand 1982). A new model and interpretation by Romani & Yadigaroglu (1995) suggest that optical and other high energy emission come from the last open field lines above one pole in an outer potential gap (Cheng, Ho, & Ruderman 1986) and exhibits the same observed polarization sweep. Since the radio MP and IP align with the high energy components, their radio emission also comes from the outer gap above one pole, and the highly polarized precursor originates above the polar cap on the opposite side of the pulsar.

The profiles do exhibit some apparent symmetry in the placement of components. In Figure 3, we have arranged average profiles in a polar plot from 8.4 GHz in the inner circle to 0.33 GHz in the outer circle. One can easily see the phase shift of the IP from 1.4 to 4.7 GHz, and the near  $180^\circ$  separation between the low frequency IP and the line denoting the phase of the LFC. However, the pulse profile does not appear to be symmetric about this line. The only symmetrical features we can derive from this plot are the MP and IP pair, and the HFC1 and HFC2 pair. Though the bisectors of these two pairs of components are less than  $180^\circ$  apart, there seems to be a physical symmetry. At low frequency, the MP and IP have nearly the same phase separation and spectral index; a common feature shared by the HFC components at high frequency. If the MP and IP originate in the outer magnetosphere as suggested by Romani & Yadigaroglu, then the HFC components may also originate in a similar region, but on a separate emitting surface with a smaller opening angle.

## 6. Conclusion

In a multifrequency study of the Crab pulsar, we have found new and unusual components that defy explanation by emission from a simple dipole field geometry. Two of the new components have a flatter spectrum than the main pulse and interpulse, and so they survive to become visible

at high radio frequencies, possibly even at infrared energies. The interpulse is replaced between 2.7 and 4.7 GHz with a new component exhibiting a much different spectrum. And a new component found 36° ahead of the main pulse may be a leading conal component to the core emission of the precursor. We are making polarimetric observations at frequencies higher than 1 GHz of the new components to understand their emission and location in the Crab's magnetosphere. We find that the occasional “giant” pulses from the Crab are emitted mostly at the phase of the MP and less often at the IP, but never at the phases of the other components. Since there seem to be no “giant” pulses at optical or  $\gamma$ -ray wavelengths where the emission is incoherent (Lundgren 1994), the giant pulse phenomenon must be related to the degree of radio emission coherence, rather than energetic particle production. The emission region conditions must, therefore be similar at the MP and IP, but the LFC, HFCs, and precursor must be significantly different.

The VLA is part of the National Radio Astronomy Observatory, which is operated by Associated Universities Inc., under a cooperative agreement with the National Science Foundation. The Arecibo Observatory is part of the National Astronomy and Ionosphere Center, which is operated by Cornell University under contract with the National Science Foundation. This work has been conducted with partial support of NSF grant AST-9315285. DAM acknowledges the support of NRAO as a Junior Research Fellow, and also thanks D. Nice of NRAO for software support and advice during the data reduction process of this project. We thank J. Rankin for valuable background information and discussion of the results, and we thank J. Gil for a provocative review.

## REFERENCES

Boynton, P. E., Groth, E. J., Hutchinson, D. P., Nanos, G. P., Jr., Partridge, R. B., and Wilkinson, D. T. 1972, *ApJ*, 175, 217

Cheng, K. S., Ho, C., and Ruderman, M. A. 1986, *ApJ*, 300, 522

Comella, J. M., Craft, H. D., Lovelace, R. V. E., Sutton, J. M., and Tyler, G. L. 1969, *Nature*, 221, 453

Cordes, J. M. 1980, *ApJ*, 237, 216

Cordes, J. M. 1978, *ApJ*, 222, 1006

Frail, D. A. 1995, private communication

Groth, E. J. 1975, *ApJS*, 29, 431

Hankins, T. H. and Moffett, D. A. 1996, (in preparation)

Hankins, T. H., and Fowler, L. A. 1986, *ApJ*, 304, 256

Harnden, F. R., Jr., and Seward, F. D. 1984, *ApJ*, 283, 279

Kristian, J., Visvanathan, N., Westphal, J. A., and Snellen, G. H. 1970, *ApJ*, 162, 475

Kuz'min, A. D. 1992, in *Proceedings of IAU Colloquium 128*, ed. T. H. Hankins, J. M. Rankin, and J. A. Gil (Pedagogical University of Zielona Góra Press:Poland), p. 2

Lundgren, S. C., Cordes, J. M., Beckwith, S. V. W. 1995, private communication

Lundgren, S. C. 1994, Ph.D Thesis, Cornell University

Lyne, A. G., and Pritchard, R. S. 1994, *Jodrell Bank Crab Pulsar Timing Results Monthly Ephemeris*

Lyne, A. G., and Pritchard, R. S. 1995, private communication

Lyne, A. G., Pritchard, R. S., and Smith, F. G. 1988, *MNRAS*, 233, 667

Manchester, R. N., and Johnston, S. 1995, *ApJ*, 441, L65

Manchester, R. N., and Taylor, J. H. 1977, *Pulsars* (San Francisco:Freeman), p. 59

Manchester, R. N., Huguenin, G. R., Taylor, J. H. 1972, *ApJ*, 174, L19

Manchester, R. N. 1971, *ApJS*, 23, 283

Narayan, R., and Vivekanand, M. 1982, *A&A*, 113, L3

Percival, J. W., Biggs, J. D., Dolan, J. F., Robinson, E. L., Taylor, M. J., Bless, R. C., Elliot, J. L., Nelson, M. J., Ramseyer, T. F., van Citters, G. W., Zhang, E. 1993, *ApJ*, 407, 276

Radhakrishnan, V., and Cooke, D. J. 1969, *Ap.Lett.*, 3, 225

Rankin, J. M. 1993, *ApJ*, 405, 285

Rankin, J. M., Comella, J. M., Craft, H. D., Richards, D. W., Campbell, D. B., Counselman, C. C. 1970, *ApJ*, 162, 707

Romani, R. W., and Yadigaroglu, I.-A. 1995, *ApJ*, 438, 314

Sieber, W. 1973, *A&A*, 28, 237

Staelin, D. H. and Reifenstein, E. C. 1968, *Science*, 162, 148

Stinebring, D. R., Kaspi, V. M., Nice, D. J., Ryba, M. F., Taylor, J. H., Thorsett, S. E., and Hankins, T. H. 1992, *Rev. Sci. Inst.*, 63, 3551

Taylor, J. H., and Weisberg, J. M. 1989, *ApJ*, 345, 434

Thorsett, S. E. 1991, *ApJ*, 377, 263

Ulmer, M. P., Lomatch, S., Matz, S. M., Grabelsky, D. A., Purcell, W. R., Grove, J. E., Johnson, W. N., Kinzer, R. L., Kurfess, J. D., and Strickman, M. S. 1994, *ApJ*, 432, 228

Vandenberg, N. R., Clark, T. A., Erickson, W. C., Resch, G. M., Broderick, J. J., Payne, R. R., Knowles, S. H., and Youmans, A. B. 1973, *ApJ*, 180, L27

Wielebinski, R., Jessner, A., Kramer, M., Gil, J. A. 1993, *A&A*, 272, L13

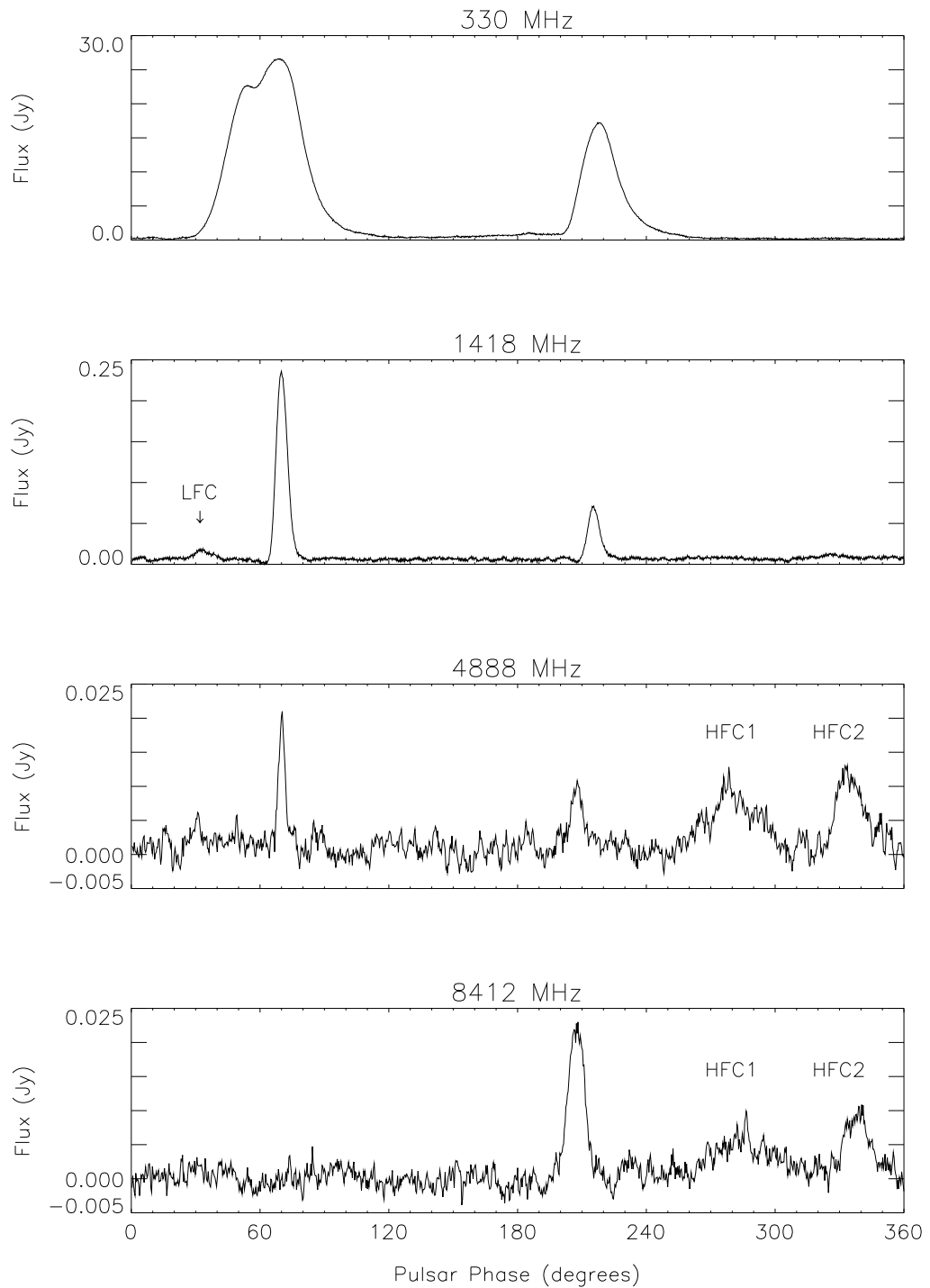


Fig. 1.— Aligned VLA profiles of the Crab pulsar.

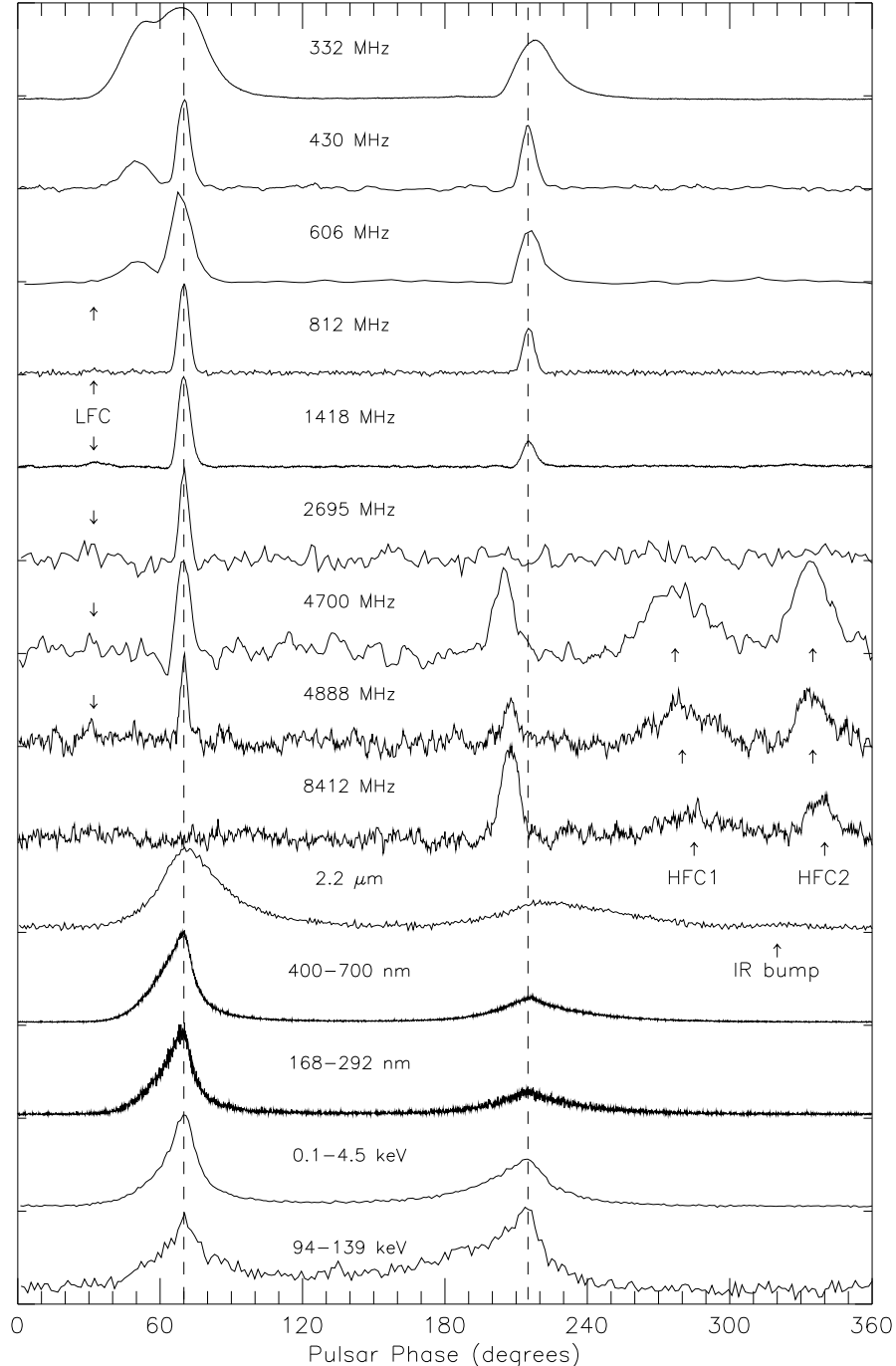


Fig. 2.— A summary of Crab pulsar profiles. 332, 430, 606, 1418, 2695, 4700, 4888 and 8412 MHz: this work; 812 MHz, 2.2 $\mu$ m: Lundgren, Cordes, & Beckwith (1995), 400-700 and 168-292 nm: Percival et al. (1993); 0.1-4.5 keV: Harnden & Seward (1984), 94-139 keV: Ulmer et al. (1994).

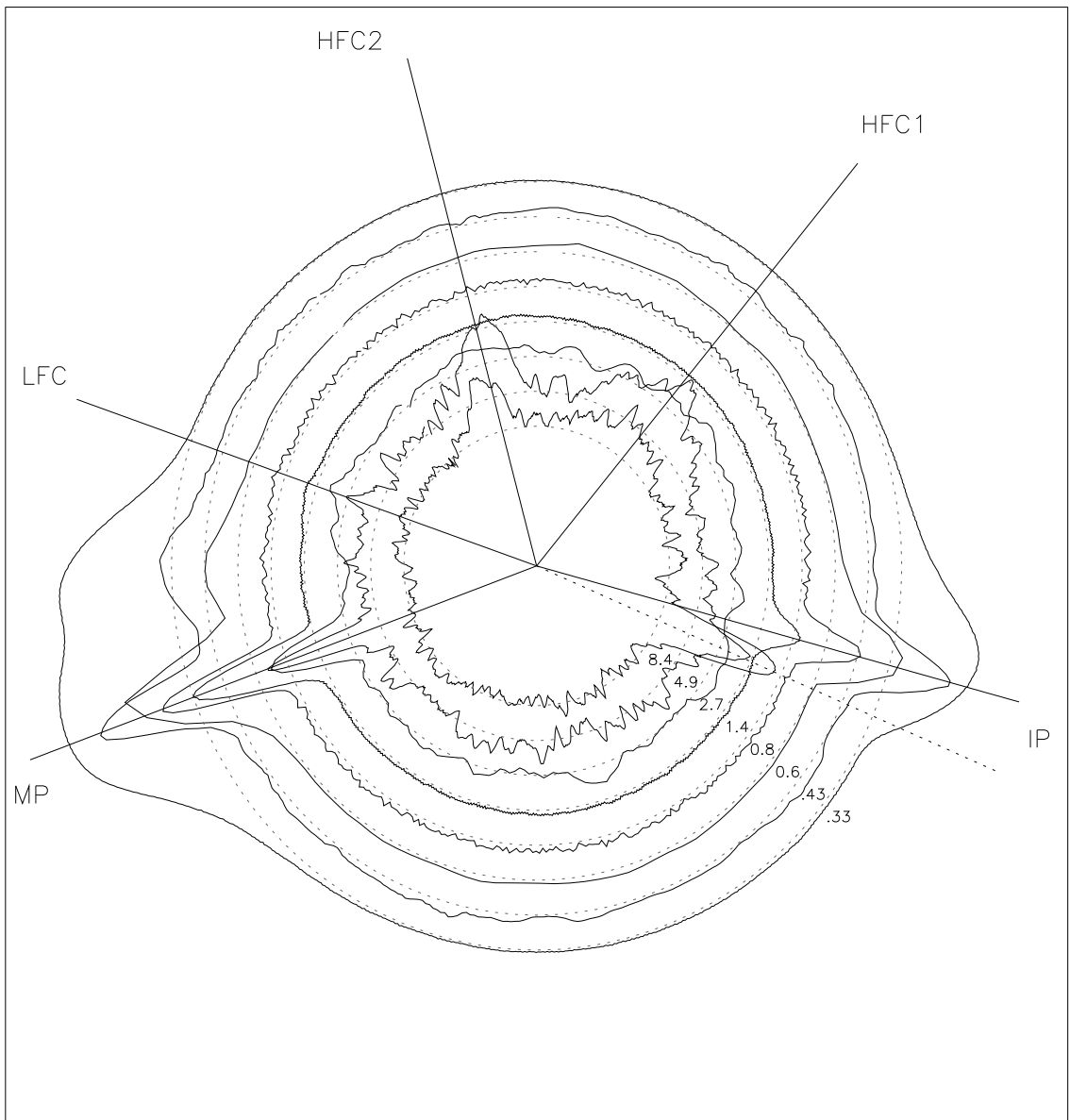


Fig. 3.— A polar plot of Crab pulsar profiles at radio frequencies shown in Figure 2. Frequencies in radial order: 8412, 4888, 4700, 2695, 1418, 812, 606, 430 and 332 MHz.